CMS Draft Analysis Note

The content of this note is intended for CMS internal use and distribution only

2014/11/01
Head Id: 168171
Archive Id: 163790:265506MP
Archive Date: 2013/01/29
Archive Tag: trunk

Search for long-lived neutral particles decaying to photons with missing energy in proton-proton collision at $\sqrt{s} = 8$ TeV

Shih-Chuan Kao, Yuichi Kubota, Tambe Norbert, and Roger Rusack
University of Minnesota

Abstract

A search for long-lived neutral particle (neutralino) decaying into photon and an undetectable gravitino is performed using 19.1 fb^{-1} of proton-proton collision data at $\sqrt{s} = 8\,\text{TeV}$. We present a method which exploits its long-lived feature by using the time measurement from the CMS ECAL detector. The method is sensitive in a range of lifetime ($c\tau$) between 0.7 and 10 m with nearly free standard model background. Taking GMSB as a benchmark model and applying our method to data, no significant excess is observed above background expectation. An exclusion region of neutralino mass and lifetime at 95% C.L. is set by using CLs method.

1 Introduction

The observation of the new neutral boson at LHC provides strong evidence for the existence of the standard model higgs and encourages the search for the physics beyond the Standard Model. What is left from the standard model are the fine-tuning problems and the unification of gauge coupling and gravity. With solutions for both questions, supersymmetry has been one of the popular theories beyond the standard model. In addition, the LSP (Lightest Supersymmetry Particles) in supersymmetry can be a stable particle and is a good the candidate for dark matter and further motivates the searches for SUSY evidence.

In the GMSB (Gauge Mediated Suppersymmetry Breaking) model [1] which provides a viable mechanism to break the supersymmetry, gravitino ($\tilde{G}$) is the LSP. Under the assumption of R-parity conservation, it is stable, and all other supersymmetry particles will promptly decay to NLSP (Next-to-Lightest Supersymmetry Particle) and then NLSP decay into gravitino and SM particles. Different parameters suggest different candidates for NLSP such as neutralino ($\tilde{\chi_0}$), stau or sneutrino. The choice of SUSY breaking scale has significant impact on the decay modes and the lifetime of NLSP.

If the neutralino is the NLSP, it has three different channels, photon, Z boson or higgs. The decay width for each channel depends on the choice of SUSY parameters. In this study, we choose the 'snowmass Points and Slopes 8' (SPS8) [2] scenario as our search phase space. In this scheme, the neutralino decays to a photon and a gravitino has the largest branching ratio [3]. Its lifetime is proportional to

$$\tau \propto \frac{M_P^2 m_{\tilde{G}}^2}{m_{\tilde{\chi_0}}^5} \tag{1}$$

where M_P is Plank mass. The neutralino mass ($m_{\tilde{G}}$) and the gravitino mass ($m_{\tilde{\chi_0}}$) are related to the SUSY breaking scale Λ.

$$m_{\tilde{G}} = \frac{c_{grav}\Lambda M}{\sqrt{3}M_p} \tag{2}$$

In this equation, M is messanger's mass and c_{grav} is a free parameter to tune the gravitino mass to adjust the lifetime of neutralino at a given scale. In this search, we focus on non-prompt decays with different neutralino lifetime ($c\tau$) from several tenth of a meter 10 meters at different SUSY breaking scale.

The neutralino are mainly produced when squarks or gluinos are pair produced. The cascade decay chain of a squark or gluino will lead to a neutralino NLSP. Depending on the branching ratio of photon channel, the final state of event should contains one or two photons and missing energy from un-detectable gravitino.

Since the hypothetic neutralino is long-lived and its mass is not trivial, its time of flight can contribute significant delay with respect to prompt produced photon. With fine granularity and great energy and timing resolution, CMS electromagnetic calorimeter (ECAL) becomes an useful tool to search delay photon signal from long-lived neutral particles decay.

On the other hand, there is no direct physics process from TeV level proton-proton collisions showing the delayed timing in current scheme of the Standard Model. Therefore, the use of ECAL timing provides a search with nearly zero background. In this study, we not only use

timing from ECAL but also explore the features of topological parameters of cluster shape to search long-lived neutral particle decaying to photon.

2 Data and Monte Carlo samples

The data used in the analysis was collected during 2012 runs with integrated luminosity of 19.1 fb^{-1}. The dataset is summarized in table 1. EXODisplacedPhoton dataset is the collection by requiring events pass displaced photon trigger in single photon dataset. Isolated Photon50 samples contain events pass single isolated photon trigger (HLT_Photon50_CaloIdVL_IsoL) with HLT photon object p_T greater than 50 GeV. This sample is used for the study of displaced photon trigger efficiency. The cosmics ray data sample are used for background study. The signal Monte Carlo (MC) samples are generated by `PYTHIA 6` [4] with an extenal SLHA (Supersymmetry Les Houches Accord) file which describe SUSY parameters and mass spectrum. The generation for signal samples adopts SUSY GMSB scheme where the SUSY breaking scale (Λ), and c_{grav} are varied to cover an appropriate range (150 mm to 10000 mm) of neutralino lifetime. Since neutralino lifetime is not a direct parameter in the SLHA configuration, the actual lifetime of the sample is obtained by fitting $c\tau$ distribution of the sample. For the SUSY breaking scale, Λ, it ranges from 100 TeV to 180 TeV in this analysis.

For the background, there is no specific process which causes the real time delay from the collisions. Therefore, a complete data-driven background estimation is used in this analysis. The $\gamma+$ jets samples are the simulation of photon radiated from a quark in QCD process. The events were generated in different p_T spectrums with respect to the quark (denoted as $\hat{p_T}$). This sample is just used for timing calibration and resolution study. The samples from Monte Carlo simulation are listed in table 2 and table 3.

Dataset Name	Recorded Luminosity [fb^{-1}]
`Run2012B-EXODisplacedPhoton-22Jan2013-v1`	5.1
`Run2012C-EXODisplacedPhoton-19Dec2012-v1`	6.9
`Run2012D-EXODisplacedPhoton-19Dec2012-v1`	7.1
`/Run2012C/Cosmics/Run2012C-22Jan2013-v1/RECO`	3130384 (events)
`/Run2012D/Cosmics/Run2012D-22Jan2013-v1/RECO`	52430 (events)
`Isolated Photon50B` `/Run2012B/SinglePhoton/Run2012B-22Jan2013-v1/RECO`	3554489 (events)
`Isolated Photon50C` `/Run2012C/SinglePhoton/Run2012C-22Jan2013-v1/RECO`	4334874 (events)

Table 1: The dataset name and corresponding integrated luminosity of the data used in the analysis

Λ (TeV)	$c\tau$ (mm) from fitting									
100	212	425		1691	1691	1691	2870	3941	5860	9285
120	161	323	645	1282	1933	2558	2937	3961	5948	10242
140	130	515	1021	1542	2047		2899	3927	6061	10154
160	243	485		970		1952	2933	3912	4932	10023
180	182	365	734	1093	1475	2202	2959	4087	5863	10352

Table 2: The signal GMSB MC samples used in this analysis

$\hat{p_T}$	σ_{LO} (pb)	number of events
$50 \sim 80$	3322.3	1995062
$80 \sim 120$	558.3	1992627
$120 \sim 170$	108.0	2000043
$170 \sim 300$	30.1	2000069
$300 \sim 470$	2.1	2000130
$470 \sim 800$	0.212	1975231

Table 3: The $\gamma+$ jets samples used in this analysis

3 ECAL Time

The ECAL Time is the main observable from the signal in this study. The time measurement is determined from the raising edge of the pulse shape from the readout of the Avalanche Photo-Diode (APD) of ECAL detector. Since an ECAL cluster of a photon object contains many crystals, we examed two different timing information in order to find out the most accurate way to retrieve timing information of the photon and reject the background, which are listed below.

- Seed time: ECAL Time form the seed crystal of the seed basic cluster of photon object.
- Cluster time: The weighted averaged time from all crystals in the seed basic cluster (equation 3). A normalized χ^2 cut ($\chi^2 < 4$) is imposed.

$$T_{cluster} = \frac{\sum_i t_i \times \frac{1}{\sigma_i^2}}{\sum_i \frac{1}{\sigma_i^2}} \tag{3}$$

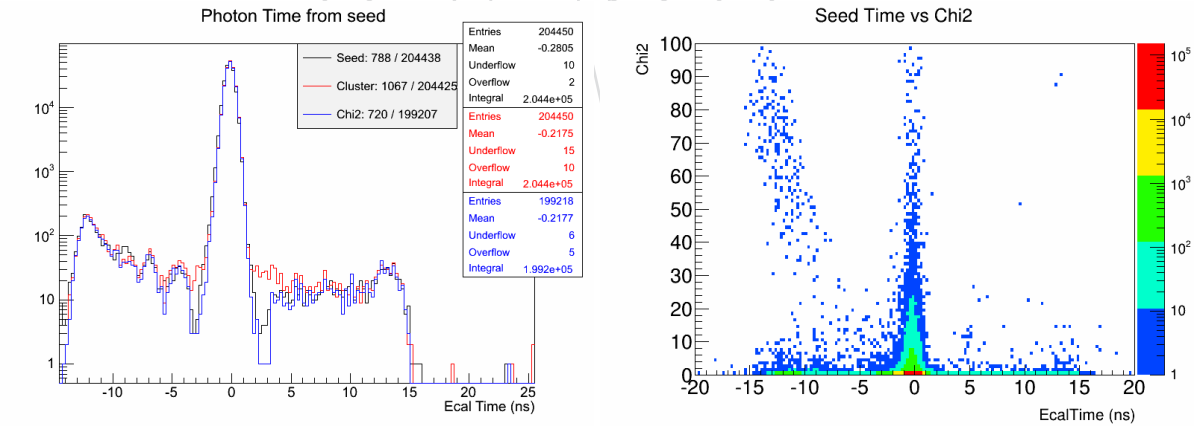

Figure 1: Different timing distributions from background control events (0 and 1-jet evebts). It shows that χ^2 cut can reduce the off-time photons

According to their performance, seed time and cluster time both have similar central value and resolution. We choose seed time of photon because seed time could possibly reveal the nature of sources for the photon object. For example, an ECAL spike signal along with pileup contribution could form a fake out-of-time photon object. Nevertheless, the normalized χ^2 cut ($\chi^2 < 4$) is still used in photon object selection. It can potentially remove fake photon objects from pile-up effect.

Another use of the cluster time is to address the time of a jet since its electromagnetic components usually doesn't belong to a single particle. As shown in figure 2, jet time and photon time are correlated and all jet time are within 3 ns window. This is a cross-check that both objects are from the same bunch crossing. Moreover, it also support thats a fake photon object from a jet or any QCD contamination is still in regular timing window.

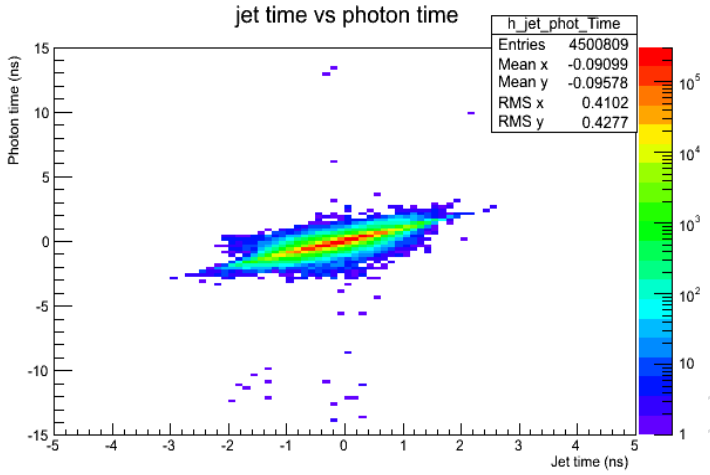

Figure 2: The jet and photon time correlation

The long lifetime of neutralino is the main reason of the delay timing which results in the photon decayed away from primary vertex. It implies that the delay is either from the slow motion of neutralino or non-trivial decay angle with respect to the neutralino momentum. Two quantities, $\Delta t1$ and $\Delta t2$, are defined to examine the contribution from both effects (figure 3) :

- $\Delta t1$ = (L1/cβ) - (L1/c)
- $\Delta t2$ = (L1 + L2 - L3)/c

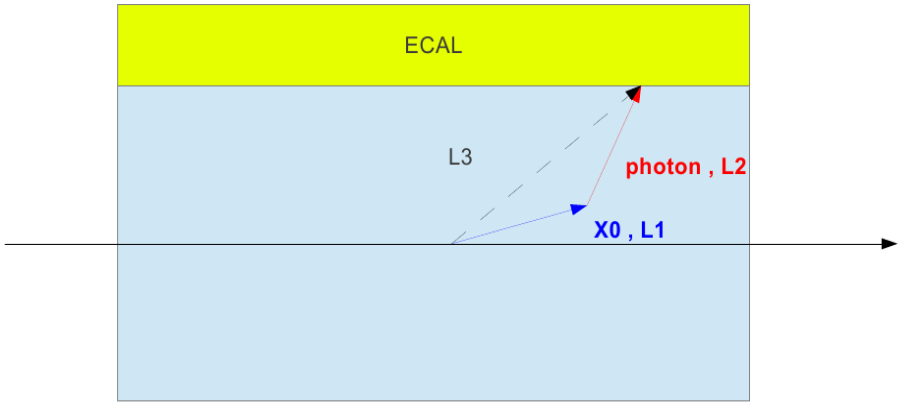

Figure 3

where L1 is the decay length of neutralino, L2 is the decay photon path and L3 is the distance between primary vertex and the signal ECAL cluster. Comparing with ECAL time, (L1/cβ) + L2/c - (L3/c), $\Delta t1$ measures the delay from the neutralino's motion and $\Delta t2$ gives the delay from the deviation of the photon path assuming neutralino is at the speed of light. The dis-

tribution of $\Delta t1$ and $\Delta t2$ from signal MC sample (figure 4) for delay photon events indicates that the slow motion of neutralino is the main cause for the delay ECAL time. Moreover, the decayed photon from neutralino is tend to move in the same direction of neutralino due to the boost of neutralino.

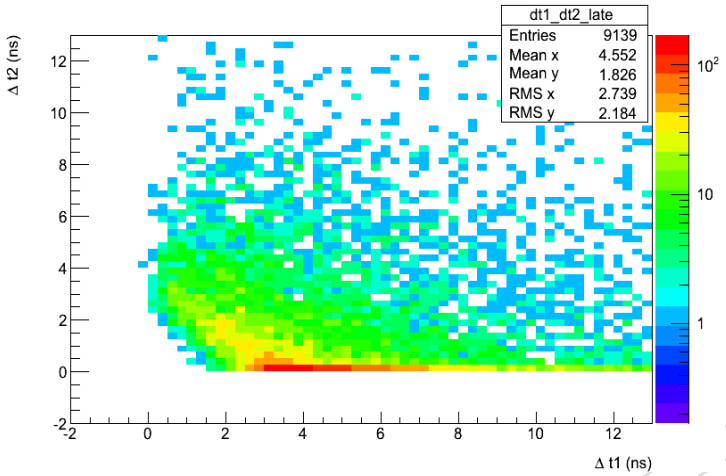

Figure 4: $\Delta t1$ and $\Delta t2$ distribution of GMSB sample (Λ 180 TeV and $c\tau$ 6000 mm)

The time resolution is measured by fitting the time distribution. A control sample from data is selected by requiring one isolated photon, one or two jets and $\not{E}_T$ less than 30 GeV in events. From $\gamma+$ jets MC samples, they are generated in a wide $\hat{p_T}$ range from 50 GeV to 800 GeV. Comparing results from MC and data, it suggests that the central value of timing from MC need to be shifted about 111 ps and an additional smearing on resolution (about 287 ps) is also required (figure 5). These valuse are then applied to the signal MC samples.

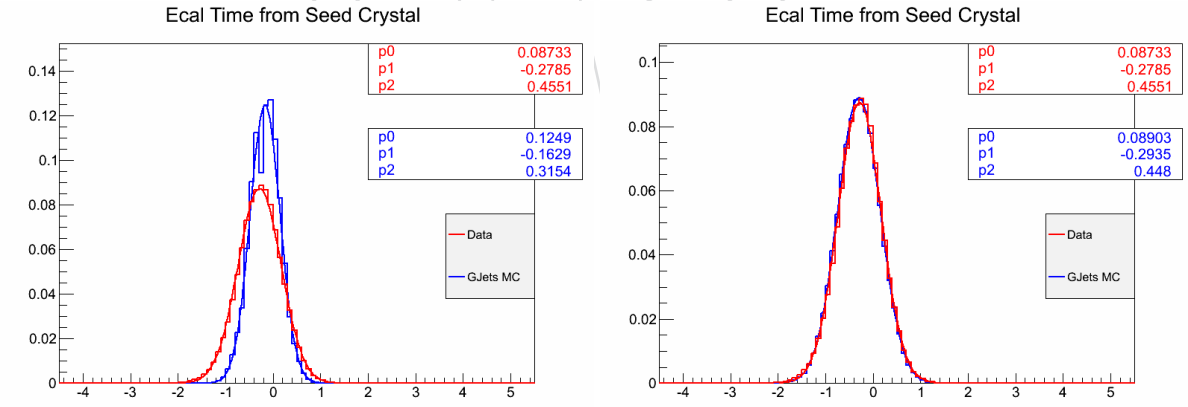

Figure 5: The comparison between time distribution between $\gamma+$ jets MC (blue) and Data (red) before (left) and after (right) calibration

4 Event and Object Selection

Since photons decayed from long-lived neutral particle is the main signature from the signal, it not only implies that the distinguishable timing difference between signal and background but also suggests that the photon does not necessarily points to the CMS interaction point. The

crystals of the CMS ECAL detector are pointing to the mean position of the primary interaction vertex which implies a round shape of ECAL cluster for photon objects from collision.

Therefore, the ECAL cluster shape also can be used to distinguish signal and background since the photon decayed from long-lived neutralino can be decayed away from primary vertex. An earlier study already demostrate the selection of off-pointing photon by using variable S_{major} and S_{minor} [5, 6], where S_{major} is the major axis and S_{minor} is minor axis of the elliptical shape of ECAL cluster. Based on the study in section 3, one major source of late photon is from slow motion of neutralino. In this scenario, the decay angle of photon from neutralino is not necessary to be large. A certain constraint on S_{major} or S_{minor} for signal selection may not be effective. In contrast, the background study shows that anomalous ECAL spiles have smaller S_{major} and S_{minor} values due to its smaller cluster size. Thus, a range of S_{major} and S_{minor} (section 5.3) is only set to exclude them.

Another common feature for long-lived neutral particles events is missing energy. Since gravitino ($\tilde{G}$) is undetectable for the CMS detector, significant amount of missing energy is expected in event topology. A cut on $\not{E}_{\mathrm{T}}$ is also useful to lower the rate from the standard model backgrounds like $\gamma+$ jets process and QCD events (Figure 6). Based on above consideration, we have concluded our on-line and off-line selection in the following sections.

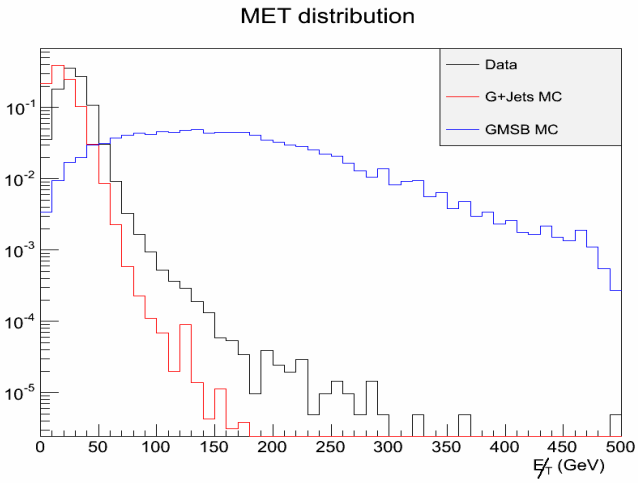

Figure 6: The $\not{E}_{\mathrm{T}}$ distribution for data and MC samples

4.1 Trigger

The events are selected online using the trigger, HLT_DisplacedPhoton65_CaloIdVL_IsoL_PFMET25. The trigger was developed to devote displaced photon analysis. In order to decrease model dependency, the trigger only requires one isolated photon with p_{T} threshold 65 GeV and particle flow $\not{E}_{\mathrm{T}}$ above 25 GeV. Based on the knowledge learned from previous 7 TeV study [6], QCD multijet events have longer tail in S_{minor} distribution and ECAL spikes tends to have smaller values. Therefore a S_{minor} constraint ($0.1 < S_{minor} < 0.4$) is implemented in order to increase the purity of real photon events (figure 7).

The efficiency and turn-on curve are studied separately for two objects, photon and $\not{E}_{\mathrm{T}}$, in trigger definition. In order to decouple correlation between photon and $E_{\mathrm{T}}^{\mathrm{miss}}$, single photon dataset (HLT_IsoPhoton50) is used for efficiency measurement. The photon in the event must pass offline selection (see next section) and its ECAL time must be within 2 ns ($|t| < 2$ ns). The photon efficiency is measured from the percetage of the HLT photon object with a matched

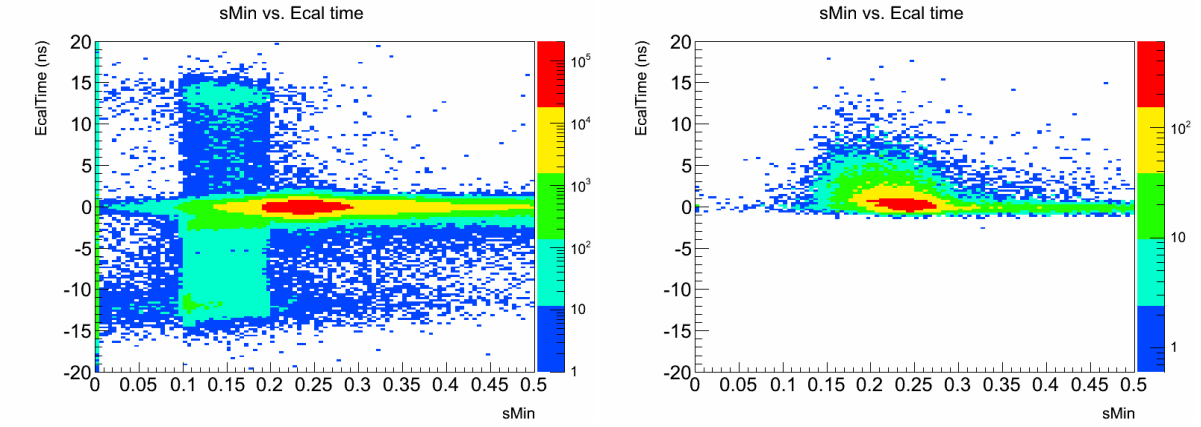

Figure 7: The S_{minor} v.s. ECAL time distribution for Data (left) and GMSB MC (right). The data sample has been pre-selected by HLT trigger

offline reconstructed photon ($\Delta R < 0.5$). Similar to photon, the efficiency of missing E_{T} is measured from the ratio of the offline PF $E_{\mathrm{T}}^{\mathrm{miss}}$ with a HLT $E_{\mathrm{T}}^{\mathrm{miss}}$ object greater than 25 GeV in the event. The result (figure 8) shows that the turn-on curve for photon will reach the plateau at p_{T} 80 GeV and 60 GeV for PF $E_{\mathrm{T}}^{\mathrm{miss}}$. A 2D efficiency (figure 9) is also examed by using signal MC samples. This is used to verify that no correlation on efficiency for photon object and PF $E_{\mathrm{T}}^{\mathrm{miss}}$.

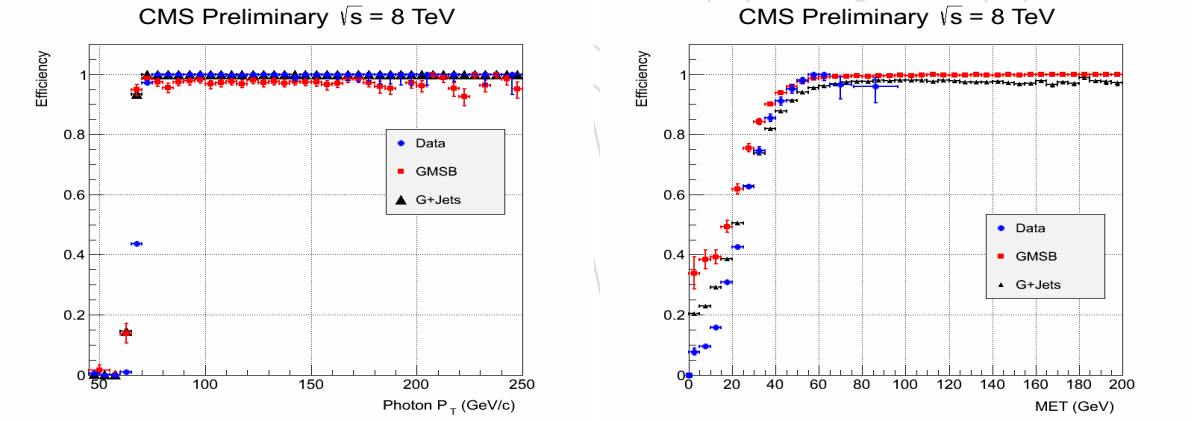

Figure 8: The trigger efficiency turn-on curve for the photon p_{T} (left) and for $\not{E}_{\mathrm{T}}$ (right). The efficiency of $\not{E}_{\mathrm{T}}$ for γ+jets is from samples with $\hat{p_{\mathrm{T}}} > 170$ GeV, which potentially contain real high $\not{E}_{\mathrm{T}}$ in the event. Contrary to $\not{E}_{\mathrm{T}}$ efficeincy, the photon p_{T} curve for γ+jets is measured from low $\hat{p_{\mathrm{T}}}$ samples ($\hat{p_{\mathrm{T}}} < 170$ GeV). Due to different sources and spectrum of $\not{E}_{\mathrm{T}}$, the turn-on curves for $\not{E}_{\mathrm{T}}$ have different slope but the plateau start at the same point around 60 GeV.

4.2 Offline Event Selection

According to the signal event topology, neutralino are pair produced from the decay of two sparticles. Therefore, at least two jets in the event final state is classified as a signal region. Zero and one jet events are considered as background dominated area which is used as a background control region for closure test of our background estimation. Due to large rate of ECAL spikes and its nature of negative timing, the normal photon reconstruction constrained the use of ECAL crystals with ECAL time in a 3 ns window ($|t_{crystal}| < 3$ns) from ECAL barrel system and 10 ns window ($|t| > 10$ ns) for ECAL endcap system. This results in a cut-off at 3 ns for

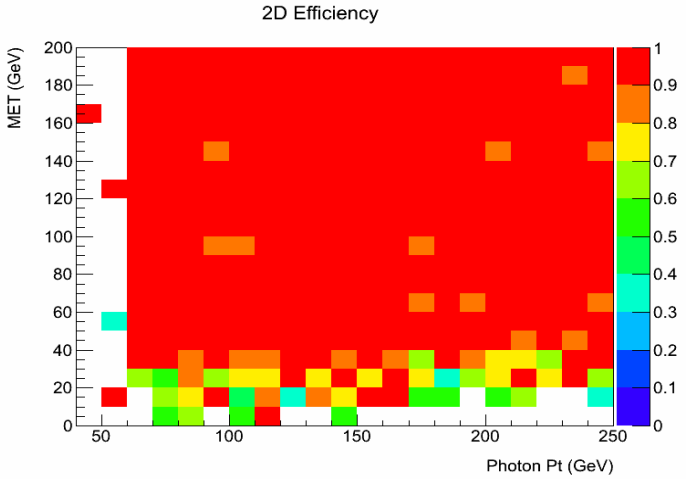

Figure 9: The HLT trigger efficiency for photon and PF $E_{\mathrm{T}}^{\mathrm{miss}}$

normal photon object. Therefore, the photon reconstruction was re-processed with the setup which extends to include those "out-of-time" crystals. However, this recovery does have the disadvantage to bring back those out-of-time machine induced background such as halo or spikes. Moreover, the energy deposits from out-of-time crystals will be considered as part of isolation energy deposit. Consequently, the out-of-time photons will not be isolated. Therefore, the isolation is not applied in the photon selection. The summary for photon selection are listed below:

- The p_{T} of leading photon is greater than 80 GeV. Other photons in the event must have p_{T} greater than 45 GeV
- Photon from ECAL Barrel, i.e. $|\eta| < 1.47$
- H/E < 0.05
- $\Delta R(track, photon) > 0.6$
- $0.12 \leq S_{minor} \leq 0.38$

For jets and $\not{E}_{\mathrm{T}}$ reconstruction, particle-flow algorithm is used because it takes tracking information into account for incomplete calorimeter measurement. With the same reason, particle-flow algorithm does not charge out-of-time photons for $E_{\mathrm{T}}^{\mathrm{miss}}$ calculation. In this analysis, we compensated the constributions from these out-of-time photons in $\not{E}_{\mathrm{T}}$ calculation and redefined it as MET2. In the offline event selection, is not required to keep event but will be used in the background estimation after certain alternations. The jet selection criteria are listed below.

- Jet $p_{\mathrm{T}} > 35$ GeV.
- Number of constituents > 1
- Charged EM energy fraction (CEF) < 0.99
- Neutral hadronic energy fraction (NHF) < 0.99
- Neutral EM energy fraction (NEF) < 0.99
- If $|\eta|$ of the jet < 2.4, charged hadronic energy fraction (CHF) > 0
- If $|\eta|$ of the jet < 2.4, charged multiplicity (NCH) > 0
- ΔR (jet, photon) $> 0{,}3$

4.3 Efficiency and Acceptance

Under the constraint of the CMS ECAL geometry, the decay length of neutralino in the CMS lab frame determines the efficiency and acceptance for reconstruction and event selection. The transverse decay length is used in this study because the radius of the ECAL is constant for different η. The efficiency of reconstruction and event selection shows that no dependence between different $c\tau$ models (figure 10a) at the same SUSY breaking scale. A clear drop around 1500 mm reflect the outter surface of ECAL detector. The time acceptance is defined as the fraction of the photons with ECAL time greater than 3 ns. Thus the higher $c\tau$ value leads to higher acceptance (figure 10b). As discussed in section 3, there are two sources of delay photons from neutralino's decay. Each one has a different acceptance with respect to decay length (figure 11) The difference can be found when separating them with $\delta t2 = 0.5$. The acceptance for slow neutralino increases with decay length monotonically but the acceptance for large decay angle case has a peak around 800 mm.

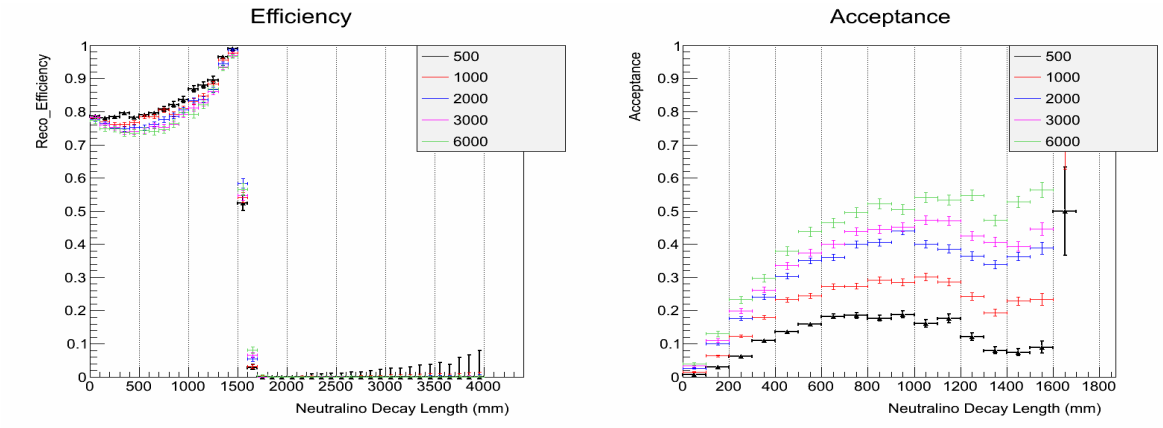

(a) (b)

Figure 10: The efficiency of reconstruction and selection and time acceptance with respect to transverse decay length in lab frame for different $c\tau$ values at *Lambda* 180 TeV.

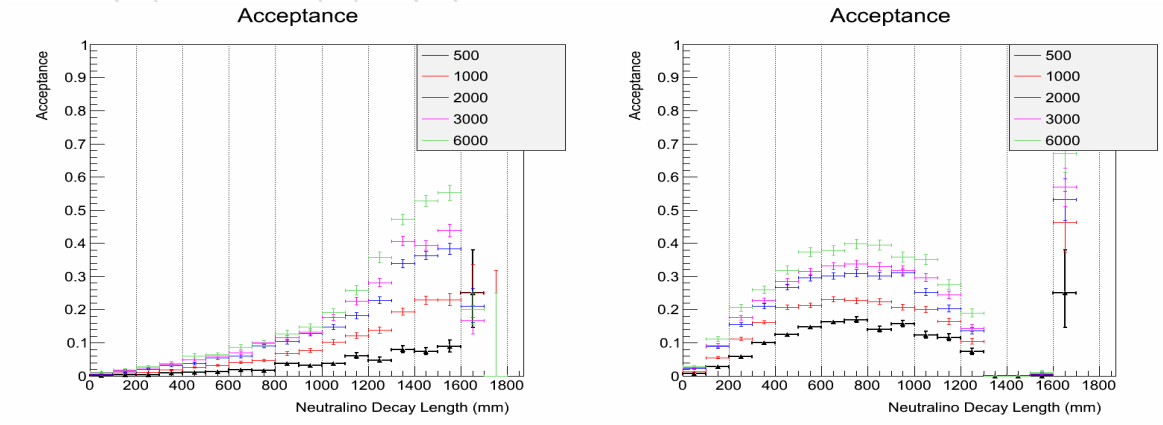

(a) (b)

Figure 11: The time acceptance with respect to transverse decay length in lab frame for late photons from slow neutralino (11a, $\Delta t2 < 0.5$) and large decay angle (11b, $\Delta t2 > 0.5$)

Since the timing depends on neutralino's decay kinematics, the total acceptance (including efficiency) should be invariant at the same proper lifetime and β if neutralino mass is the same. Figure 12 shows that the consistency among different $c\tau$ values at the same Λ scale.

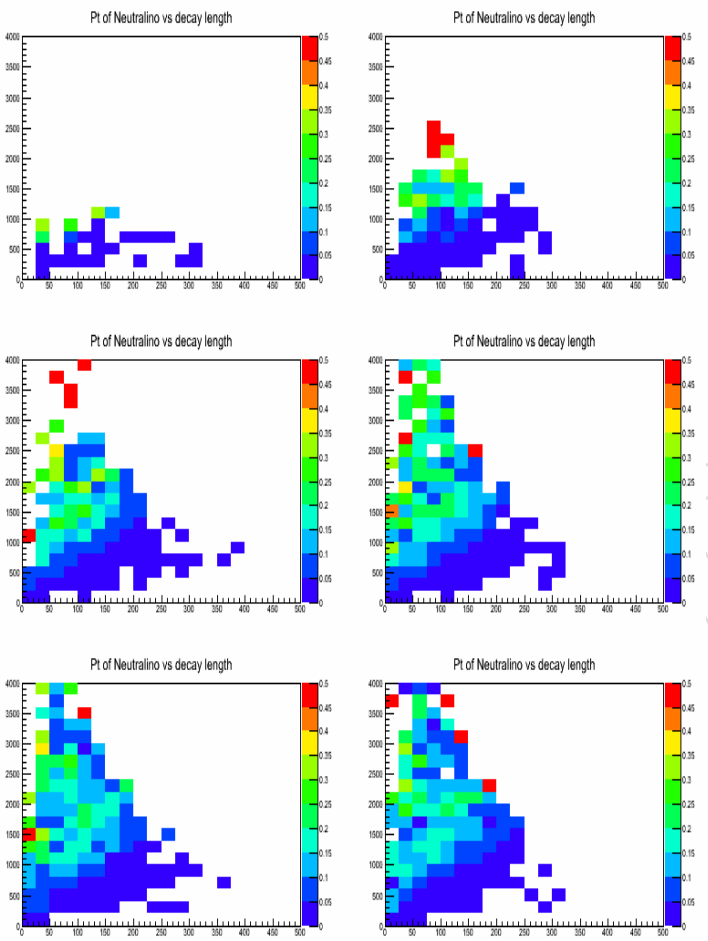

Figure 12: Efficiency $\times$ Acceptance in different $c\tau$ values at Λ 180 TeV.

The efficiency decreases at the same lifetime if the SUSY breaking scale Λ decreases. This is due to the fact that the neutralino mass is lighter. Therefore, the p_{T} and missing energy spectrum of neutralino's decay will be softer (figure 13).

5 Background Estimation

Since there is no known reaction from collisions has delayed photon production, the possible sources of background for late photon may come from bad timing measurement or fake photon objects which are not from collisions. As mentioned in previous section, ECAL time is determined by the pulse shape. Since the time from seed scrystal is adopted, the seed of photon object becomes the issue of mis-measurement of timing and indication of its source.

In order to study the background behavior, an in-time photon sample and an off-time photon sample are defined. The nominal photons have ECAL time between -1 ns and 1 ns and are from the events contain at least two jets. The off-time photons are photons with ECAL time greater than 2 ns or smaller than -3 ns with no jet in the event. By comparing with these two

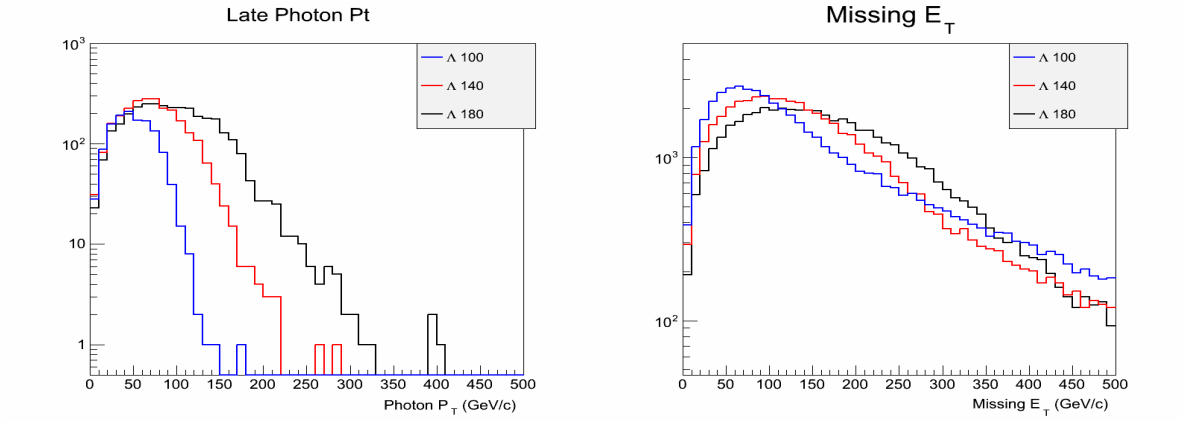

(a) (b)

Figure 13: The delayed photon p_T and E_T^{miss} spectrum from different Λ with the same $c\tau$ (6000 mm). With higher Λ, the p_T spectrum is harder.

samples, a summary of differences is listed belowed. Based on these phenomena, we classified background into three difference types, halo, anomalous ECAL spikes and cosmic-rays which are described in the following sections.

1. Clear matching between a CSC segment and their ECAL Cluster in off-time sample (Figure 14). The first bin, smallest $\Delta\phi$ has higher entries than other bins. This is due to a fact that many matched CSC segments are from muon chamber ME1/1/A. The chamber connect three strips to one readout ADC which causes two additional indistinguishable imaging segments for one segment. The chambers also locate at the similar radius as ECAL. Therefore it increases the probability to match with a ECAL cluster.

2. Different S_{Major} and S_{Minor} population. Figure 15 shows the differences between in-time and off-time photons. A normal photon cluster has simialr S_{major} and S_{minor} values since the cluster shape is round shape. The off-time samples have abnormal large S_{major} and smaller S_{minor}. According to distributions of S_{Major} with respect to η and ϕ (Figure 16), they suggests possible more than one source of background. some of them distribute around horizental plane (ϕ are 0 or π). This one is then identified as halo. The other are evenly distribute aross ϕ.

3. Matching between a DT cosmic-ray segment and a photon cluster (Figure 17). A clear matching can be seen in the off-time sample. This suggests cosmic-rays is not negligible component.

Based on these features, we defined following parameters to identify the background sources.

- CSC$\Delta\phi$, the ϕ difference between a CSC segment and a photon cluster.
- S_{Major} and S_{Minor}.
- DT$\Delta\phi$ and DT$\Delta\eta$, the ϕ and η difference between a DT cosmic-ray segment and a photon cluster.

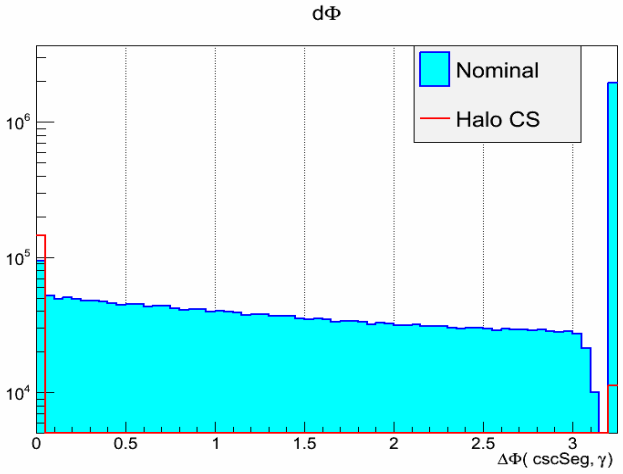

Figure 14: CSC $\Delta\phi$ distributions of in-time (blue) and off-time (red) samples. The events in last bin have no CSC segment information available.

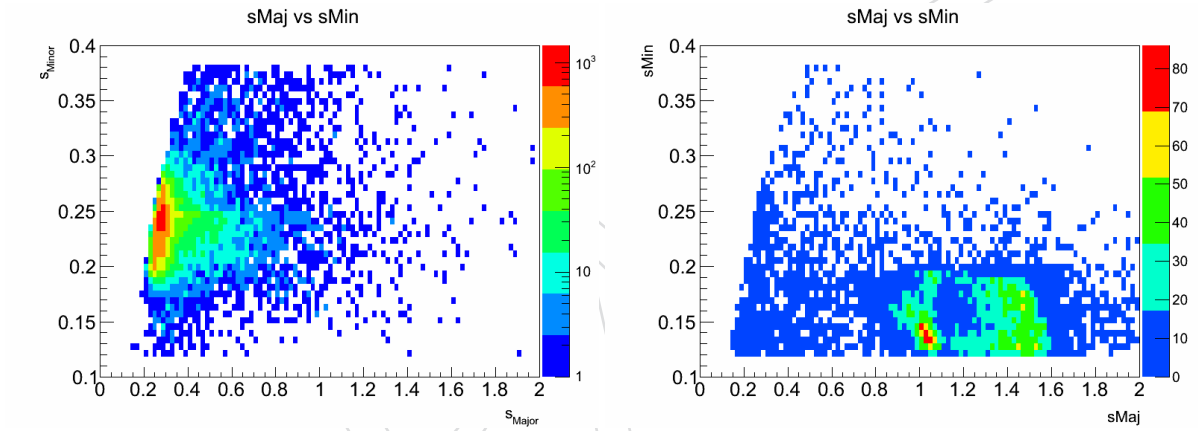

Figure 15: The comparison between nominal photon sample (left) and off-time photon sample (right) for S_{Major} and S_{Minor}

5.1 Halo Photon

Beam halo muons are known existing particles created by collsions of beam gas or scratching collimator from beams while some of them hit and bremsstrahlung in the CMS ECAL detector which create photon like objects. Since they are created by halo muons, a possible muon track can be found in the Endcap muon system. Our study shows that a clear matching between a CSC segment and ECAL cluster is found (Figure 14). Additionly, the flying path of halo muons are nearly parallel to the beam which result in a different, long ellipse shower shape which is corresponding to a larger S_{Major} and smaller S_{Minor}.

A simple approximation for the ECAL time from halo photons can be derived from

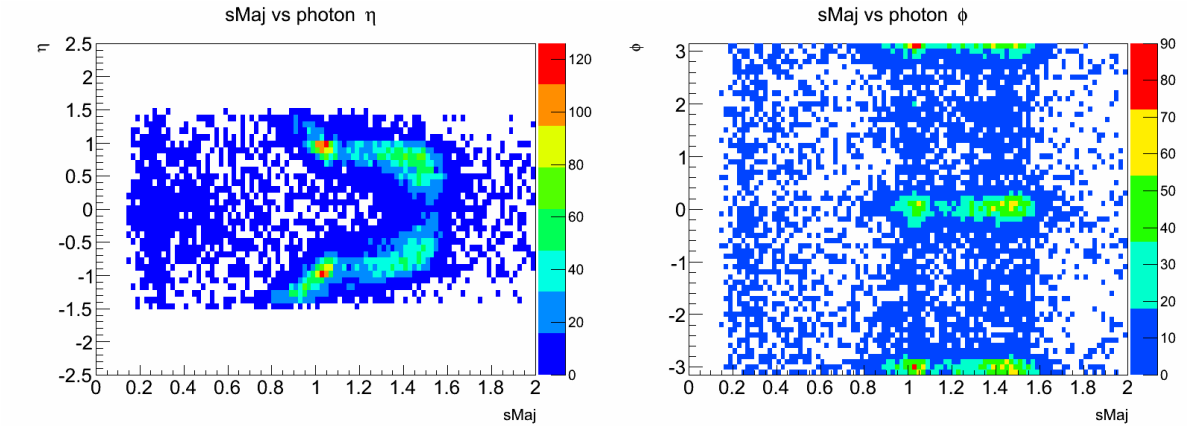

(a) (b)

Figure 16: S_{Major} distributions of off-time sample

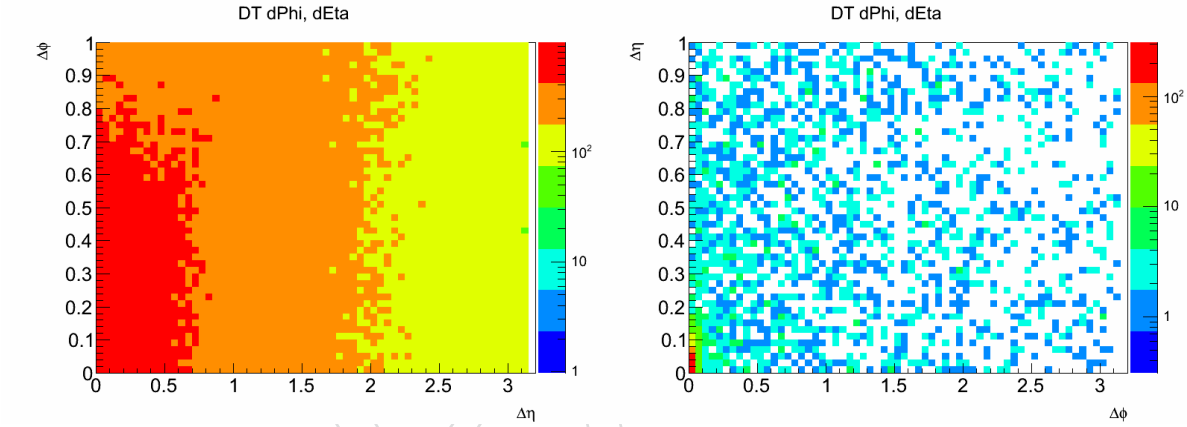

(a) In-time (b) Off-time

Figure 17: DT $\Delta\eta - \Delta\phi$ distributions of in-time (left) and off-time (right) photon samples.

$$t_0 = \frac{r}{c} = \frac{\rho}{sin\theta}\frac{1}{c} \tag{4}$$

$$t_{halo} = \frac{z}{c} = \frac{\rho}{tan\theta}\frac{1}{c} \tag{5}$$

$$t_{ECAL} = t_{halo} - t_0 \tag{6}$$

$$= \frac{\rho}{c}\left(\frac{1}{tan\theta} - \frac{1}{sin\theta}\right) \tag{7}$$

$$= -\frac{\rho}{2c}tan(\theta/2) = -\frac{\rho}{2c}\exp^{-\eta} \tag{8}$$

where ρ is the transverse radius with respect to beam pipe, r is the distance between vertex and photon cluster, z is the z position of the photon cluster, c is the speed of light, θ is azimuthal angle. The reference time (t_0) is the function of η. This equation is under the assumption that halo muons travel parallel to the beam. The ECAL time for halo photons is the time with respect to t_0, the time assumed that the ECAL cluster is orignated from primary vertex. Therefore, the

ECAL time of halo photons is a function of η and ealier than the time of photons from the associated bunch crossing.

Due to 400 MHz RF frequency of the LHC, it provides 9 more LHC buckets for proton fills. The satellite bunches are thus formed by the causes of beam captured in incorrect locations at each stage of beam transfering. The existence of satellite bunch halo can be observed from the Endcap ECAL system and identified by selecting the photon cluster matched with a CSC segment. A clear patten in 2.5 ns can be seen (Figure 18). Consequently, the halo from later arrival satellite bunches could bring late photons.

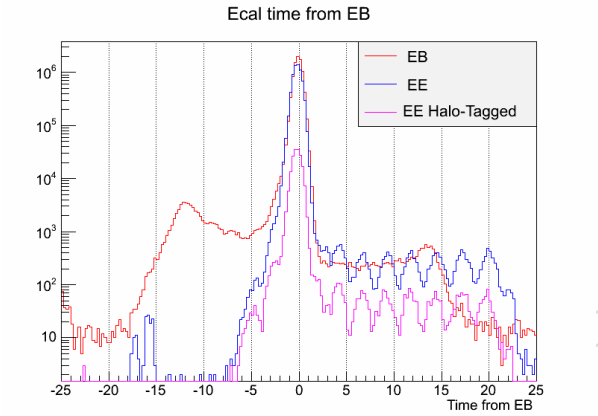

Figure 18: The ECAL time of photons from EB and EE. The periodic pattern is from the halo of satellite bunches.

Based on this estimation, a halo sample can be extracted by using this equation (Figure 19).

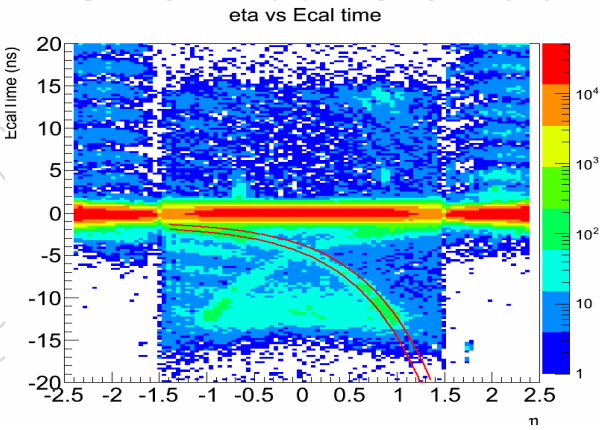

Figure 19: The η v.s. ECAL time for photons. The red curves show the fitting range to select halo control sample.

After cross examing various variables, a halo control sample can be refined by adding following criteria:

- The ϕ of the candidate must be around 0 or π ($|\phi - 0| < 0.2$ or $|\phi - \pi| < 0.2$).
- ECAL time of the halo candidate must be less than -3 ns.
- 0-jet events.

Using this control sample, we verified that the matching between a CSC segment and an ECAL

cluster is the main character of halo photons. Additionaly, it also shows the long ellipse shape of ECAL cluster, large S_{Major} and small S_{Minor}, because the shower was developed along the flight path of the halo muon, which is across crystals. Therefore, two rules to identify halo photon were concluded as

- $\Delta\phi$ between a CSC segment and a photon cluster must be smaller than 0.05.
- $0.8 < S_{Major} < 1.65$ and $S_{Minor} < 0.2$.

and its efficiency can be determined by using this control sample. Mis-tagging rate can be obtained from nominal sample (Figure 20). The mis-tagging rate is measured using the $\gamma+$ jets like events (at least two jets and $\not{E}_T < 60$ GeV) with ECAL time $|t| < 1$ ns. According to the halo control sample, S_{major} shows the dependency on η (figure 16a). Thus the efficiency and mis-tagging rates for halo component are evaluated in 5 different $|\eta|$ slices from 0 to 1.47. In this study, only the CSC$\Delta\phi$ constraint is applied to reject halo background. This is because S_{major} and S_{minor} distribution from signal MC also show significant population in the same area (figure21).

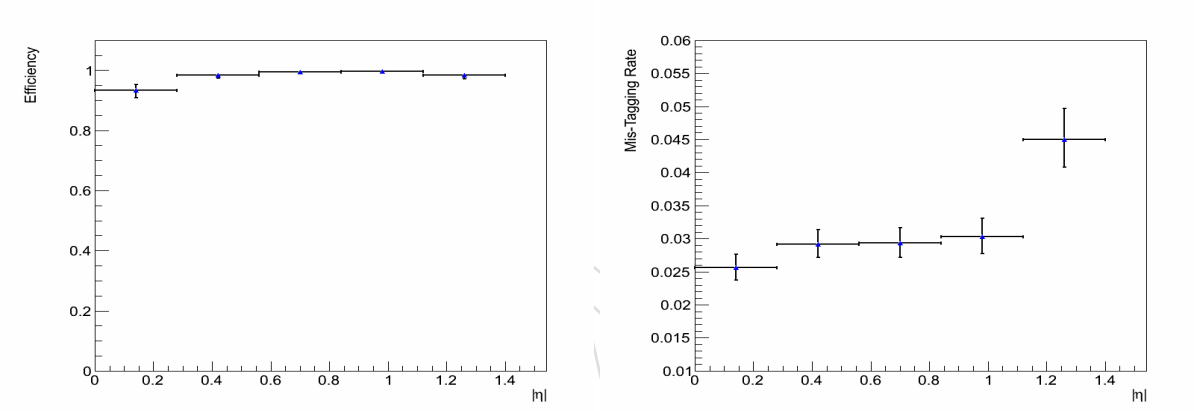

Figure 20: Tagging efficiency and mis-tagging rate for halo photons in 5 η regions

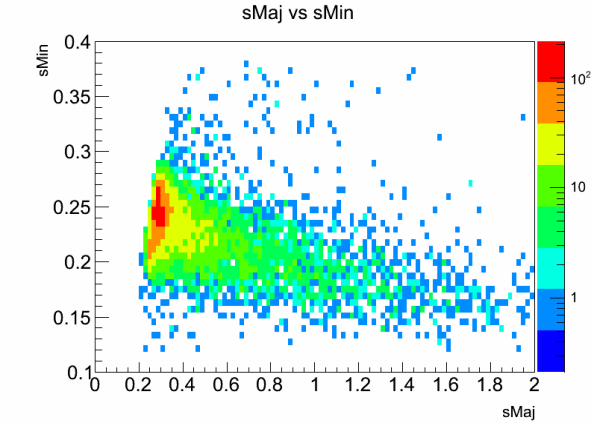

Figure 21: S_{major} and S_{minor} distribution from signal MC with cτ 6000 mm and Λ 180 TeV.

5.2 Cosmic-Ray

Similar to halo photons, cosmic-rays can possibily initiate showers in the ECAL. Their existence can be found by looking at the $\Delta\phi$ and $\Delta\eta$ between a DT cosmic-ray muon segment and an

ECAL cluster. Due to the space between Muon Barrel system and ECAL, the actual DT positon used is projecting the position of DT segment to ECAL surface from its direction. A clear match at small $\Delta\phi$ and $\Delta\eta$ can be found from off-time photon sample (Figure 17b) in contract to in-time sample (Figure 17a).

A support study for this matching method using cosmic dataset is also performed (Figure 22). Since the contain of cosmic dataset is different from collision data, event selectin criteria for cosmic data use ECAL supercluster instead of reconstructed photon object and the seed crystal energy of the supercluster must be greater than 10 GeV. A 75.5% of the cosmic tagging rate is obtained while at least one DT segment and one ECAL supercluster are both presented in the the events. A 1.4% of fake rate for this method is obtained by using the good photon control sample from diplaced photon dataset where the events pass the regular event selection and the ECAL time must be within 1 ns window ($|t| < 1$ ns).

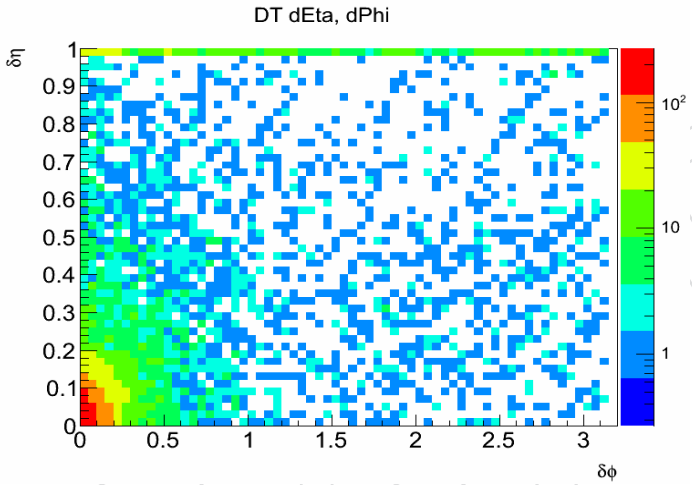

Figure 22: The $\Delta\eta$ and $\Delta\phi$ distribution of DT segment and ECAL supercluster for cosmic-ray data.

5.3 Anomalous ECAL Spike

ECAL spikes is known to be the energy deposit to the Avalanche Photo-Diode (APD) from direct ionization of charged particles from collisions [7]. Although the topological "swiss-cross" method is implemented in the reconstruction process to remove them, some of them are still observed due to its high rate. This component can be extracted from the negative timing sample where no correlation is found from other detectors such as muon endcap or muon barrel system for halo and cosmic-ray muons.

Due to its forming mechanism, its ECAL cluster size is expected to be smaller than the size of regular photons (Figure 23) and mostly has negative ECAL time because of its rapid rising edge of the signal pulse. Therefore, the second component in S_{Major} distribution (Figure 16), the smaller S_{Major} value without η or ϕ structure, can be addressed as the presence of ECAL spike. Based on their characters, the tagging criteria for spike candidate are defined below.

- Swiss-cross value < 0.9.
- $S_{Major} < 0.6$ and $S_{Minor} < 0.17$.

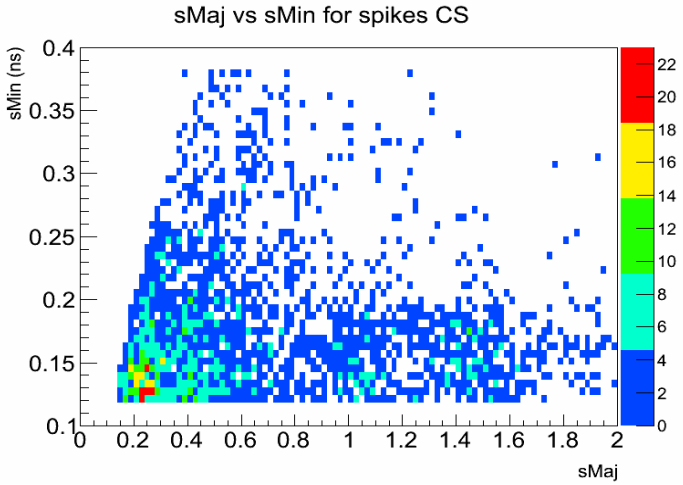

Figure 23: S_{Major} and S_{Minor} distribution of spike control sample.

5.4 ABCD Method for Un-Tagged Background and QCD

By applying above three background taggings, the ECAL timing distribution is checked from an inclusive data sample. (figure 24). The plot shows three major background components. Halo contributes the most in the off-time area. Cosmic-rays and ECAL spike background also have legitimate shape from the tagged components. However, the survived photons after removing all the tagged backgrounds still have significant amount in late timing area ($|t| > 3$ ns) . Therefore, an ABCD method is developed in order to estimate the final contamination in the signal region.

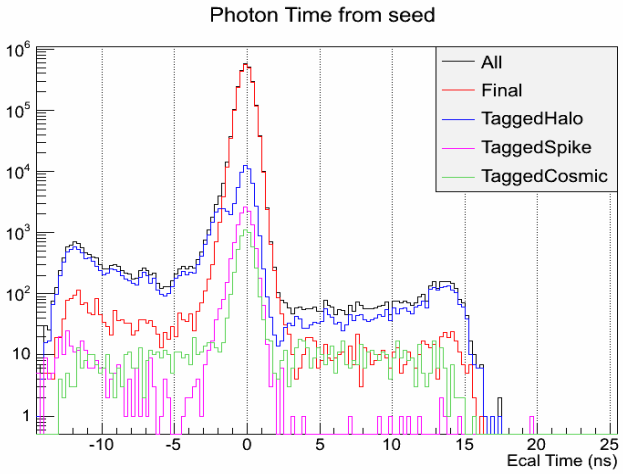

Figure 24: ECAL time distribution with

The two parameters are used in this ABCD method, ECAL time and missing transverse energy. In this analysis, the missing transverse energy from particle flow recontruction is adopted. However, the particle flow algorithm take the photons into account if the photon object from EB has ECAL time within 3 ns window and the photon from EE has ECAL time within 10 ns window.

Therefore, two different missing transverse energy are defined in term of the contribution from photons. Regardless timing of the photon object, MET1 is the missing transverse energy with-

out counting photon's contribution in the event. MET2 is the convention definition of missing transverse energy but includes out-of-time photons as part of the event. Therefore, the out-off-time photons ($|t| > 3$ns in EB and $|t| > 10$ ns in EE) should added in the calculation. In other words, MET2 is the inverse vector sum of MET1 and all photon's p_T.

According to MET1 and MET2 definations, non-collision backgrounds such as halo, spikes and cosmic-rays would have higher MET2 but small MET1 since the photon objects do not belong to the events. On the other hand, the collision backgrounds spread in MET2, small MET2 refer to QCD type of events, events with large MET2 could be from W, Z or top quark productions. However, collision events would mostly have large MET1 since the topology of selected events mostly requires at least one photon and the photons are not account for MET1 calculation. (Figure 25)

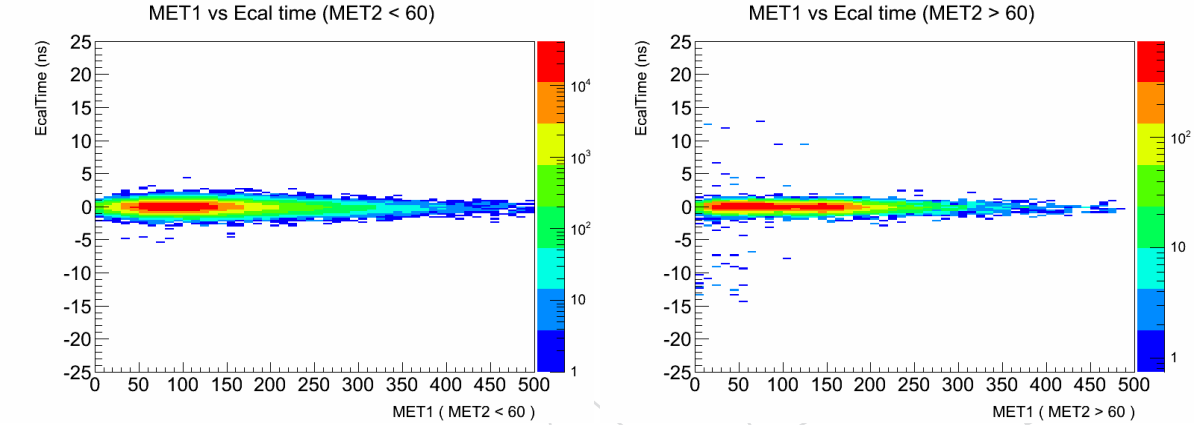

Figure 25: MET1 v.s. ECAL Time distributions for MET2 < 60 GeV (left) and MET2 > 60 GeV (right) events.

The ABCD regions are defined from ECAL time and MET1 which is shown in table 4. A and B regions are signal free region since their $|t|$ is less than 3 ns. Region C is also signal free and non-collision enhanced because events contain photon from collision should mostly have large MET1. Thus, the non-collision background in signal region D can be estimated from

$$\text{Un-tagged background in D} = \frac{B}{A} \times C \tag{9}$$

As for possible contemination from collision events, an another ABCD method using ECAL time and MET2 is developed. Since ECAL time from collision type events should be around zero, the $|t| < 2$ns region can be acted as control region for extracting background behavior. The definition of this QCD estimation ABCD is shown in table 5 and the collision background in D region can be estimated by

$$\text{Collision background in D} = \frac{F}{F'} \times D' \tag{10}$$

Similar to the collision background in D, the same formula also applicable to A,B and C regions. By substracting the QCD contributions in A,B and C regions, it provides purer un-tagged background estimation. Combinition all the estimation. The final background can be determined by

$$\text{Total background in D} = (\frac{B - Q_b}{A} \times C) + Q_d \quad (11)$$

$$Q_d = \frac{F}{F'} \times D' \quad (12)$$

$$Q_b = \frac{F}{F'} \times B' \quad (13)$$

MET2 $>$ 60 GeV	MET1 $<$ 60 GeV	MET1 $>$ 60 GeV
$t >$ 3 ns	C	D
$\|t\| <$ 2 ns	E	F
$t <$ -3 ns	A	B

Table 4: ABCD definition for un-tagged non-collision backgrounds

MET1 $>$ 60 GeV	MET2 $<$ 60 GeV	MET2 $>$ 60 GeV
$t >$ 3 ns	D′	D
$\|t\| <$ 2 ns	F′	F
$t <$ -3 ns	B′	B

Table 5: ABCD definition for collision background in B and D region

A closure test is done by using 1-jet events. The results can be found at table 6 and table 7. After applying the number in each region, the estimated background in D region for 1-jet events events is 3.62 ($^{+2.55}_{-3.04}$) which is compitable with observed value 7. The uncertainty from collision background has trivial effect because the ratio F/F′ is small.

$$\text{D} = (\frac{4 - 0.13}{11} \times 10) + (0.1) = 3.62^{+2.55}_{-3.04} \quad (14)$$

$$Q_d = \frac{30447}{1187230} \times 4 = 0.10 \pm 0.91 \quad (15)$$

$$Q_b = \frac{30447}{1187239} \times 5 = 0.13 \pm 1.13 \quad (16)$$

MET2 $>$ 60 GeV	Spikes	Halo	Cosmic	Un-tagged	Sum
D	0	1	12	7	20
C	0	17	9	10	36
B	0	10	0	4	14
A	1	44	0	11	56
F	-	-	-	-	30477

Table 6: Closure test for 0 and 1-jet events

The final background estimation from events with more than 1-jet is 0.046 ($^{+0.136}_{-0.136}$). Only one event is observed in signal region.

5.5 Cross-Check From Z Events

A cross-check for collision events is done using $Z \rightarrow e^+e^-$ events. This study uses Z mass spectrum and its sideband to extract Z events and the background sample. Since Z decays

MET2 $<$ 60 GeV	Spikes	Halo	Cosmic	Un-tagged	Sum
B′	0	1	2	5	8
D′	0	0	0	4	4
F′	-	-	-	-	1187230

Table 7: Closure test for 1-jet events

MET2 $>$ 60 GeV	Spikes	Halo	Cosmic	Un-tagged	Sum
D	0	0	0	1	1
C	0	2	0	0	2
B	3	1	1	0	5
A	0	6	0	6	12
F	-	-	-	-	30242

Table 8: Final background estimation for at least 2-jet events

promptly, the timing from the electrons must be in-time. The majority of the background is Drell-Yan process, which also have in-time electrons in the final state. However, any off-time electron could also pass event selection and present in the Z mass spectrum as well (Figure 26). Therefore, the time distribution from the Z mass sideband provides a background template with proper scale of two background sources, Drell-Yan and random electro pairs.

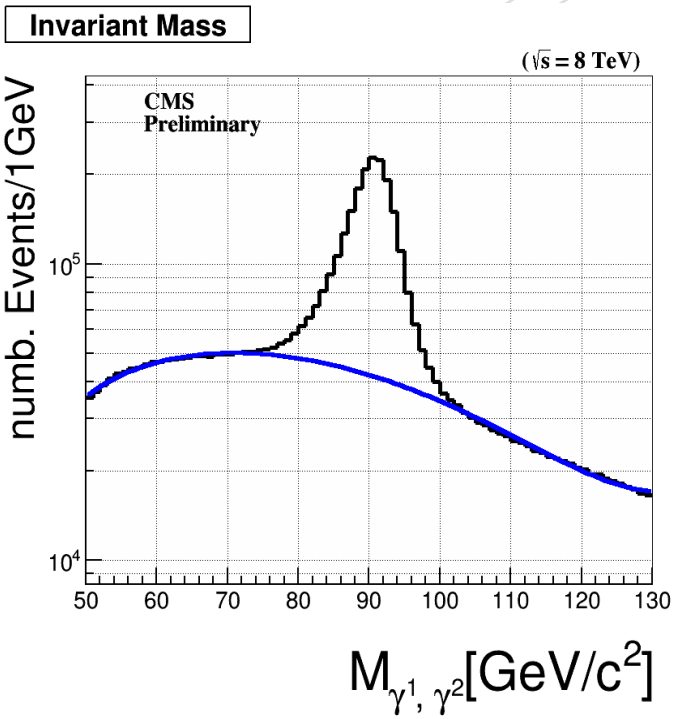

Figure 26: The invariant mass of two electrons

The events requires at least two electrons with p_{T} greater than 30 GeV. The electron isolation is not applied due to the algorithm take off-time ECAL crystal into account of isolation deposit. The Z sample is chosen by requiring the invariant mass between 76 GeV and 100 GeV of two leading electrons (Figure 27a). For the background template, the sample is from events with invariant mass between 50 to 76 GeV and 100 to 130 GeV (Figure 28a). By fitting the sideband in Z mass spectrum using a polynomial function, the background contamination in the Z sample

MET2 < 60 GeV	Spikes	Halo	Cosmic	Un-tagged	Sum
D′	0	0	0	1	1
B′	0	0	0	5	5
F′	-	-	-	-	657662

Table 9: Final background estimation for at least 2-jet events in QCD control region

area can be estimated and the background template can be normalized accordingly.

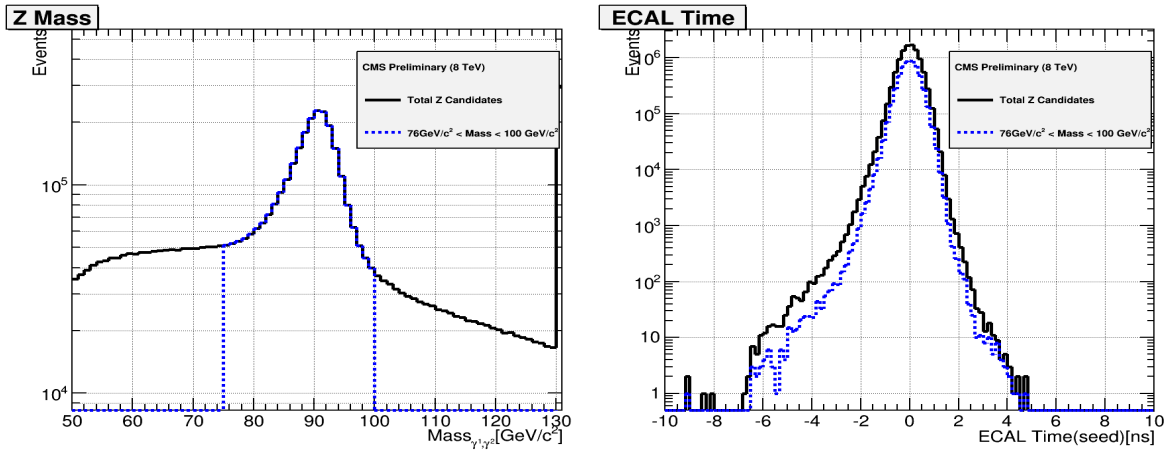

(a) (b)

Figure 27: The mass range (76 GeV $<$ *Mass* $<$ 100 GeV) and time distribution for Z candidate

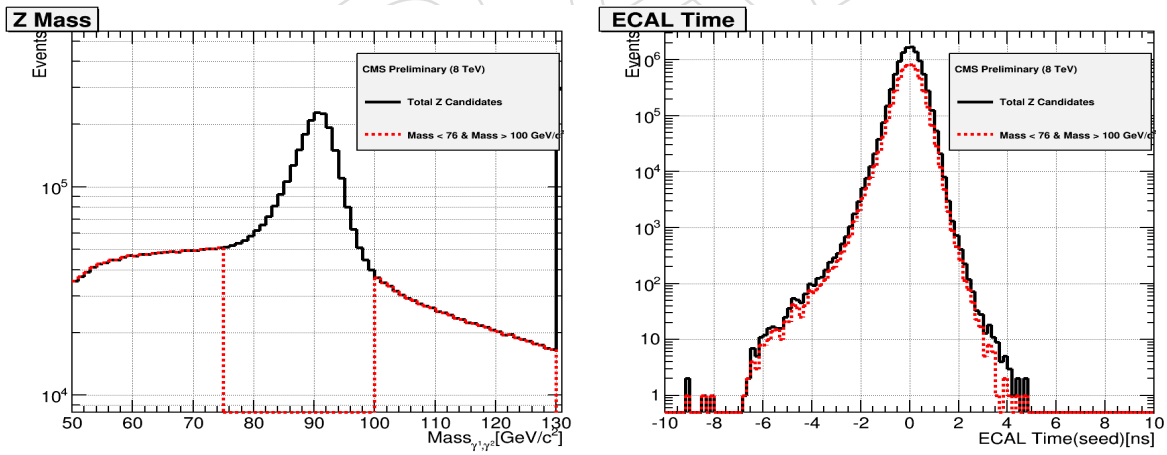

(a) (b)

Figure 28: The sideband (50 GeV $<$ *Mass* $<$ 76 GeV and 100 GeV $<$ *Mass* $<$ 130 GeV) and time distribution of background control sample.

By subtracting this background time distribution from the Z sample's , a time distribution of pure Z events can be obtained (figure 29). Based on this pure Z time distribution, a ratio (0.000007) of $|t| < 2$ ns and $t > 3$ ns can be obtained. This ratio then apply to the number from F region defined in previous section (30242) in order to verify the estimation of collision

background in D region. This method estimates 0.21 photons in D region which is consistent with the result (0.046 ± 0.136) from the ABCD method.

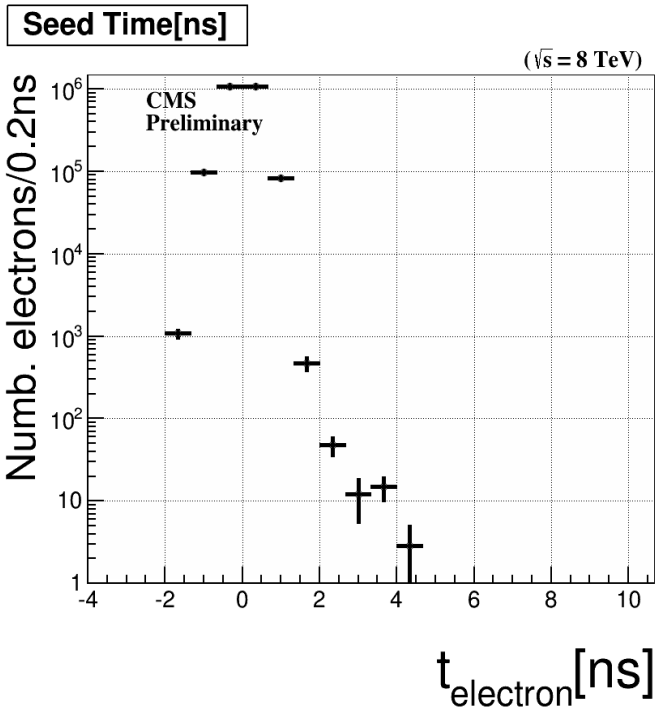

Figure 29: The time distribution of Z events

6 Systematic Uncertainties

This analysis involve photon, jet and $E_{\mathrm{T}}^{\mathrm{miss}}$ in the event topology. Thus following factors are taken into account for systematic uncertainty which are jet energy scale, jet energy resolution, egamma energy scale, unclustered energy for $E_{\mathrm{T}}^{\mathrm{miss}}$ as well as photon timing resolution. Their major impacts to the analysis is mainly on signal efficiency. Because the background estimation is a pure data-driven method, most effects from these sources are cancelled out ($< 1\%$ impact). We variated their 1-σ deviation with respect to the nominal values. The results are summarized in table (10). The time zero has most significant impact to the result since our method is a pure counting method on ECAL time. The second largest uncertainty comes from unclustered energy uncertainty of $E_{\mathrm{T}}^{\mathrm{miss}}$. It has biggest effect on $E_{\mathrm{T}}^{\mathrm{miss}}$ scale than other factors such as jet or photon energy scale. Other general factors such as luminosity and parton distribution function are adopted from the official study. These factors are all then applied in the statistic analysis as nuisance parameters.

7 Result

A search for long-lived neutral particle decaying to photon and gravitino is performed by using the data with an integrated luminosity 19.1 fb^{-1} from the LHC proton-proton collision at 8 TeV central-of-mass energy in 2012. With no significant observation exceeding above background expectation, an exclusion region for current GMSB model is set at 95% C.L. (Figure 30) by using CLs method. The result shows that ECAL timing method has sensitivity to long-lived

Source	Uncertainty(%)
time zero	6
Unclustered Energy	5
ECAL time resolution	3
Jet energy scale	2
Jet energy resolution	1
Photon energy scale	1
Luminosity	2.6
PDF	< 1

Table 10: Systematic uncertainties for signal efficiency

neutralino between $c\tau$ 500 mm and 10000 mm. By scanning the possible SUSY breaking scale, the exclusion region covered a range of SUSY breaking scale (Λ) between 100 TeV and 180 TeV.

Comparing with previous searches [8] [9], the CMS ECAL timing method provides broader search spectrum both for neutralino's lifetime and for the SUSY breaking scale.

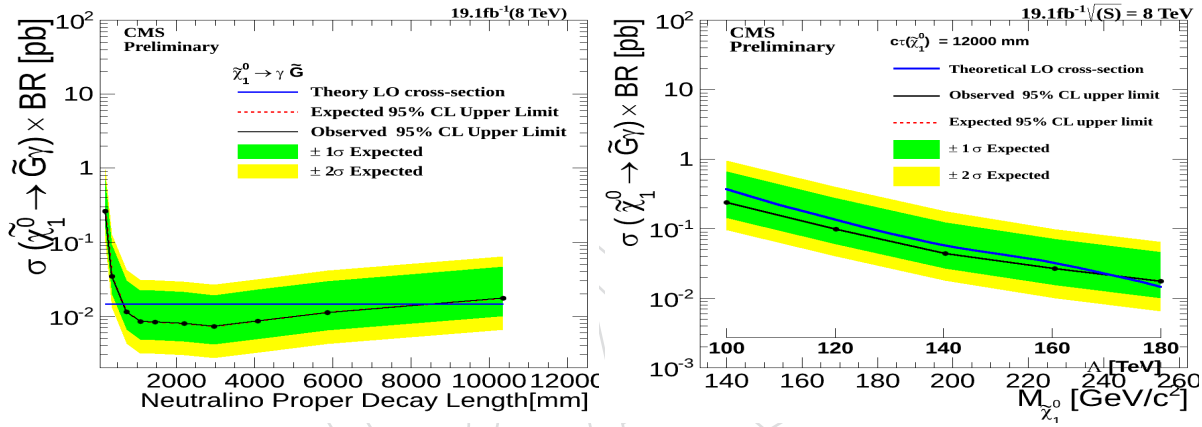

Figure 30: The upper limit at 95 % C.L. for Λ 180 TeV in different $c\tau$ and $c\tau$ 12000 mm in different Λ values using CL_s method

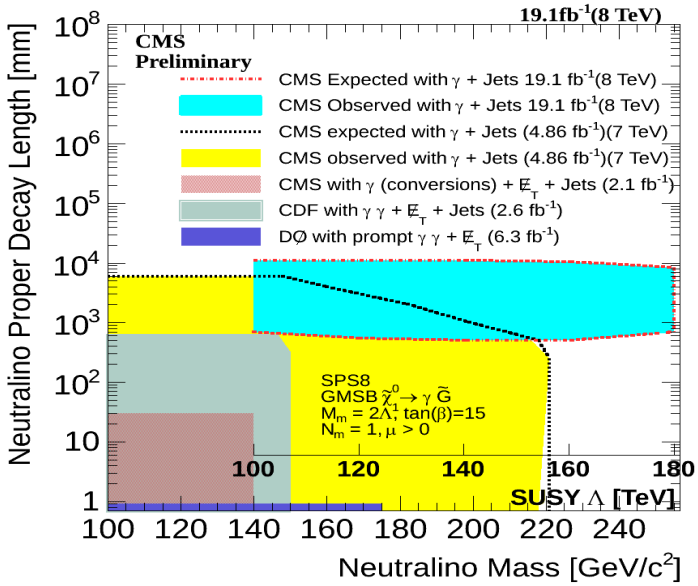

Figure 31: The exclusion region for the mass and lifetime of neutralino in the SPS8 model

References

[1] G. F. Giudice and R. Rattazzi, "Theories with Gauge-Mediated Supersymmetry Breaking", *Phys. Rep.* **322** (Jan, 1998) 419–499. 103 p.

[2] B. C. Allanach et al., "The Snowmass Points and Slopes: Benchmarks for SUSY Searches", *Eur. Phys. J. C* **25** (Feb, 2002) 113–123. 12 p.

[3] L. Covi et al., "Gravitino Dark Matter and general neutralino NLSP", *J. High Energy Phys.* **11** (Aug, 2009) 003. Comments: 30 pages, 15 figures, pdflatex.

[4] T. Sjöstrand, S. Mrenna, and P. Skands, "PYTHIA 6.4 physics and manual", *JHEP* **05** (2006) 026, doi:10.1088/1126-6708/2006/05/026, arXiv:hep-ph/0603175.

[5] D. d. R. D. Franci, S. Rahatlou, "An algorithm for the determination of the flight path of long-lived particles decaying into photons", *AN-10-212* (2010).

[6] M. S. Daniele Del Re, Shahram Rahatlou and L. Soffi, "Search for Long-Lived Particles using Displaced Photons in pp Collisions at $\sqrt{s}$ = 7 TeV", *AN-11-081* (2012).

[7] CMS Collaboration, "Characterization and treatment of anomalous signals in the CMS Electromagnetic Calorimeter", *AN-10-357* (2011).

[8] CDF Collaboration Collaboration, "Search for Supersymmetry with Gauge-Mediated Breaking in Diphoton Events with Missing Transverse Energy at CDF II", *Phys.Rev.Lett.* **104** (2010) 011801, doi:10.1103/PhysRevLett.104.011801, arXiv:0910.3606.

[9] CMS Collaboration Collaboration, "Search for long-lived particles decaying to photons and missing energy in proton-proton collisions at $\sqrt{s} = 7$ TeV", *Phys.Lett.* **B722** (2013) 273–294, doi:10.1016/j.physletb.2013.04.027, arXiv:1212.1838.